

Enhancement in Hydrogen Storage Capacities of Light Metal Functionalized Boron–Graphdiyne Nanosheets

Tanveer Hussain^{1,*}, Bohayra Mortazavi², Hyeonhu Bae³, Timon Rabczuk²,
Hoonkyung Lee³ and Amir Karton¹

¹School of Molecular Sciences, The University of Western Australia, Perth, WA 6009, Australia

²Institute of Structural Mechanics, Bauhaus-Universität Weimar, Marienstr. 15, D-99423, Weimar,
Germany

³Department of Physics, Konkuk University, Seoul 05029, Republic of Korea

[Corresponding Author: tanveer.hussain@uwa.edu.au](mailto:tanveer.hussain@uwa.edu.au)

Abstract

The recent experimental synthesis of the two-dimensional (2D) boron-graphdiyne (BGDY) nanosheet has motivated us to investigate its structural, electronic, and energy storage properties. BGDY is a particularly attractive candidate for this purpose due to uniformly distributed pores which can bind the light-metal atoms. Our DFT calculations reveal that BGDY can accommodate multiple light-metal dopants (Li, Na, K, Ca) with significantly high binding energies. The stabilities of metal functionalized BGDY monolayers have been confirmed through *ab initio* molecular dynamics simulations. Furthermore, significant charge-transfer between the dopants and BGDY sheet renders the metal with a significant positive charge, which is a prerequisite for adsorbing hydrogen (H₂) molecules with appropriate binding energies. This results in exceptionally high H₂ storage capacities of 14.29, 11.11, 9.10 and 8.99 wt% for the Li, Na, K and Ca dopants, respectively. These H₂ storage capacities are much higher than many 2D materials such as graphene, graphane, graphdiyne, graphyne, C₂N, silicene, and phosphorene. Average H₂ adsorption energies for all the studied systems fall within an ideal window of 0.17–0.40 eV/H₂. We have also performed thermodynamic analysis to study the adsorption/desorption behavior of H₂, which confirms that desorption of the H₂ molecules occurs at practical conditions of pressure and temperature.

Keywords: 2D Materials, Material design, Hydrogen storage, H₂adsorption, H₂desorption

1. Introduction

Due to the continuous increase in global energy utilization and the effects of fossil fuel consumption on the climate, the development of sustainable and renewable energy supplies is a matter of urgency. Hydrogen (H₂) is considered an ideal alternative to the depleting fossil fuels due to attractive properties such as high energy density with no harmful effects on the environment. However, an efficient way of storing H₂ is the main obstacle towards its realization as a green and clean energy carrier.[1-4] Among different storage routes, 2D material-based H₂ storage seems to be the most sustainable option provided a suitable material is available, which meets the criteria proposed by US Department of Energy.

Carbon nanostructures (CNs) is a family of materials, which has been studied extensively for H₂ storage applications in different morphologies, such as carbon nanotubes, graphene, graphane, graphdiyne, graphyne and many others.[5-14] However, the limitation of CNs, in their pristine form, is the weak binding with H₂ molecules, which restricts their applications as efficient H₂ storage materials due to small H₂ uptake or low operating temperatures.[15] Thus, the binding energies of H₂ with the host CNs must be enhanced for storage at ambient conditions. Several techniques have been employed for improving H₂-CNs binding, e.g., spillover effect, defects formation in host materials, application of electric fields, inducing charges, and metal functionalization.[16-20]

Functionalization of CNs and other nanostructures by introducing various elements for H₂ storage has been comprehensively studied. Zhou and Szpunar investigated the H₂ storage properties of graphene sheets doped with Pd nanoclusters. They found that Pd clusters of 5–45 nm uniformly distributed over the graphene nanosheet attain H₂ storage capacity of 6.7 and 8.7 wt% at pressures of 50 and 60 bar, respectively.[21] Zhou *et al.* synthesized Ni/graphene composites in which Ni clusters of 10 nm are uniformly dispersed over the graphene surface and studied their H₂ storage capacities. At ambient conditions an H₂ storage capacity of 0.1 wt% was achieved, and it could be increased to 1.2 wt% at a pressure of 60 bar.[22]

Theoretical studies of metal functionalized CNs other than graphene for H₂ storage have also been carried out. Liu *et al.* used first principles calculations based on density functional theory (DFT) to study the structural, and H₂ storage properties of Mg doped py-graphyne sheet and obtained a storage capacity of 10.6 wt%. [23] It was reported that the application of electric field would restrict the aggregation of Mg dopants and the adsorbed H₂ molecules bind with an energy range of 0.28 eV/H₂, which falls within the desired window. Pan *et al.* used DFT calculations to study the H₂ storage properties of various CNs such as C₄₀, C₄₁, C₆₃, C₆₄ and C₆₅ doped with Ca at various concentrations. They concluded that Ca binds strongly with the CNs and anchor multiple of H₂ molecules attaining a high H₂ storage capacity of up to 8.6 wt%. [24] Another DFT study by Mohajeri and Shahsavar investigated metal functionalization of a graphyne monolayer under nitrogen and sulphur co-doping. They reported high H₂ storage capacities of 9.0 and 9.3 wt% for Li and Na metal doping, respectively. [25]

The above studies demonstrate that metal functionalization of CNs can play a vital role in improving H₂ binding with the host material. A very recent addition to the family of two-dimensional CNs is the boron-graphdiyne (BGDY) nanosheet, which has been synthesized via a bottom-up synthetic approach. [26] Among several attractive properties of BGDY such as enhanced optical, thermal stability, mechanical response, and thermal conductivity, the presence of boron centres uniformly distributed in a carbon network creates additional binding sites for metal centres. Mortazavi *et al.* studied the structural, electronic, thermal, mechanical, optical and metal storage properties of BGDY by means of DFT coupled with molecular dynamics simulations. [27] Under the application of mechanical strain, it was concluded that this porous 2D monolayer preserves superstretchability. The authors further studied the application of BGDY as high capacity anode material for Li, Na and Ca ion batteries. Motivated by the enhanced metal storage properties of BGDY, we have employed spin-polarized DFT-D3 calculations to study its potential use as a high capacity H₂ storage material. We have considered both alkali (Li, Na, K) and alkaline earth metal (Mg, Ca) dopants uniformly distributed over the BGDY monolayer, and studied their structural, electronic and H₂ storage capacities. Our simulations revealed an optimum level of metal doping concentration for efficient H₂ storage.

2. Computational details

We have carried out spin-polarized periodic boundary condition DFT calculations using the VASP code.[28,29] In these calculations, the generalized gradient approximation (GGA) PBE exchange-correlation functional has been used.[30] We have employed projector-augmented wave (PAW) method to deal with the ion–electron interactions.[31] Empirical van der Waals corrections have been included using the D3 dispersion correction of Grimme *et al.*[32] The Brillouin zone (BZ) has been sampled by Monkhorst–Pack scheme with a mesh size of $3 \times 3 \times 1$ for geometry optimization and $7 \times 7 \times 1$ for obtaining density of states.[33] A vacuum space of 20 Å has been inserted, which is large enough to evade the possible interactions between periodic images along the z-axis. In the geometry optimizations, the convergence criteria for the total energies and forces have been set at 10^{-5} eV and 0.01 eV/Å, respectively. Binding of metal dopants to the BGDY monolayer involve charge transfer mechanism, which has been studied by means of Bader charge analysis.[34] Binding energies per dopant (E_b) of metal adatoms on BGDY are calculated using the following equation:

$$E_b = \{E(\text{GDY} + nX) - E(\text{BGDY}) - nE(X)\} / n \quad (1)$$

where $X = \text{Li, Na, K, Mg, Ca}$, and $n = 1-4$. In this equation, the first, second and third terms represent the total energies of BGDY bonded with n metal dopants, pristine BGDY monolayer and metal dopants, respectively.

3. Results and discussion

The optimized structure of BGDY is shown in Figure 1. The BGDY monolayer used in this study has 14 atoms (C_{12}B_2) consisting of two types of C–C bond lengths of 1.23 Å and 1.35 Å, and a B–C bond length of 1.51 Å. The calculated lattice constant of 11.85 Å and the bond lengths mentioned above agree well with the previous study which used the more reliable hybrid GGA functional HSE06.[27] In pristine form, BGDY preserves a semiconducting behavior with a energy gap (E_g) of 0.485 eV, as evident from a total and partial density of states plots (Figure 1(c)). However, this E_g value is underestimated due to the well-known inability of the PBE

functional to calculate the exact E_g . A more accurate E_g value has been calculated by Bohayra *et al.*, using the HSE06 functional they obtained a value of 1.15 eV.[27] As the mechanical, thermal and dynamic stability of the BGDY monolayer has already been studied in Reference [27], we start by investigating its metal doping capacities.

Like most of the CNs, pristine BGDY barely binds H_2 , thus metal dopants (e.g., Li, Na, K, Mg, Ca) have to be introduced to enhance the BGDY- H_2 binding energies. The binding energies of these dopants over the BGDY monolayer should exceed their corresponding cohesive energies (E_c) to ensure a reversible doping mechanism. On the other hand, when E_c exceeds E_b clustering of metal dopants would be a more likely outcome rather than binding to a BGDY. The selection of alkali and alkaline metal dopants has been based on the fact that these light elements, having lower cohesive energies, would make uniform scattering over the BGDY monolayer. We have considered all the possible binding sites on BGDY monolayer for metal doping and compare the E_b values. The lowest E_b configurations yield E_b values of -2.95, -2.51, -2.91, -1.13 and -3.04 eV for Li, Na, K, Mg and Ca, respectively. With the exception of Mg (-1.51 eV), these E_b values are much higher than the corresponding cohesive energies of Li (-1.63 eV), Na (-1.11 eV), K (-0.93 eV) and Ca (-1.84 eV).[35, 36] Moreover, our calculated E_b values for the studied dopants are higher than those of graphenylene, phosphorene, stanene, siligraphene (SiC_7) and graphdiyne nanosheets.[5,20,37-39] This indicates the potential of BGDY as a promising metal anchoring material.

Large surface to volume ratio due to its 2D nature and big pore size enables BGDY to accommodate more metal dopants. This would assist in achieving more active sites for the incoming H_2 molecules to be adsorbed on BGDY monolayers, which would result into a large H_2 gravimetric density. However, the introduction of metal dopants on BGDY will be associated with the transfer of charge from the former to the later. Thus, electrostatic repulsion between the cationic dopants could be a concern in achieving high metal doping concentration and consequently high H_2 storage capacity. Maintaining a reasonably high distance between the two adjacent metal dopants can solve this problem. For further metal adsorption, the BGDY doped with single metal dopant has been considered as initial structure. The second dopant is introduced on all possible binding sites available on BGDY monolayer preserving a sufficiently large distance from the existing metal atom. The lowest energy structures among the considered configurations are associated with E_b values of -2.62, -2.10, -

2.45 and -2.61 eV, for Li, Na, K and Ca, respectively. Upon the introduction of second dopant, the reduction in E_b values are 11.19, 16.33, 15.80 and 14.14% for Li, Na, K and Ca, respectively. Despite the decrease in E_b , we still obtain $E_b > E_c$, which indicates that the dopants dispersion over BGDY is preferred instead of metal clustering. We kept on adding more metal dopants as long as their E_b is exceeding the E_c values. The optimized structures of BGDY monolayers with maximum metal dopants considered in this study are shown in Figure 2. For the third dopant, BGDY monolayer pre-adsorbed with two dopants and for the fourth dopant, BGDY pre-adsorbed with three dopants served as an initial structure. It is important to mention here that the minimum dopant-dopant distance at the highest doping concentrations for Li, Na, K and Ca has been found as 4.45, 5.16, 5.20 and 4.86 Å, respectively. Complete results for the structural parameters of all the systems at various doping concentrations are given in table 1. The E_b values in the case of four dopants for all the metals are still higher than their corresponding E_c as shown in Figure 3 (a).

In addition to the energetic stability, that is $E_b > E_c$, we have confirmed the thermal stabilities of BGDY monolayers loaded with four metal dopants of Li, Na, K and Ca through *abinitio* molecular dynamics simulations (AIMD). This is done by employing Nose-thermostat algorithm at 300 K for 6ps with a time step of 1fs. All the doped systems remained stable without significant structural deformation, which is evident from small variations in their energies (for further details see Figure S1 of the Supplementary Information). This ensures the thermal stabilities of metal-doped BGDY monolayers.

As mentioned above, the metal-BGDY interactions involve charge transfer, we have employed Bader analysis to estimate the amount of charge transfer between the dopants to the BGDY monolayers. At a maximum doping concentration, that is BGDY-4X (X=Li, Na, K, Ca) each Li, Na, K and Ca dopants have transferred an average charge of 0.98, 0.68, 0.60 and 1.09 e to the monolayer, respectively. This implies that BGDY monolayers attain significantly high negative charges, leaving the dopants in cationic form with reasonably high partial positive charges. Bulk share of these donated charges has been captured by the C and B atoms of the BGDY monolayer, which are in close vicinity to the dopants. Depletion and accumulation of electronic charges has been calculated by the following relation and shown in Figure 4.

$$\Delta \rho = \rho(\text{BGDY: X}) - \rho(\text{BGDY}) - \rho(\text{X}) \quad (2)$$

Here the first, second and third terms represent the charge densities of doped BGDY, pristine BGDY, and the metal dopant, respectively.

Transfer of charges from the dopants would change the electronic properties of BGDY monolayers, which have been studied by density of states plots. Figure 5 shows the partial density of states (PDOS) plot of BGDY doped with 4Li atoms. One can see a transition from semiconducting to metallic BGDY upon the introduction of Li adatoms. The contribution appearing at the Fermi level (E_f) is from Li(s), which clearly overlaps with B(p) and C(p). This Li dopant is the one, which is bonded to BGDY monolayer in the vicinity of both B and C atoms. As indicated by in the Bader charge analysis that each Li dopant donates an average of 0.98e to BGDY, thus the distinct peaks appearing between -3.70 to -3.50 eV of the left, and then 0 to 2.0 eV on the right side of E_f corresponds to Li(s) contributions to BGDY monolayer.

Similar to Li, the other dopants, Na, K and Ca, cause semiconducting to metallic transitions as shown in Figures S2–S4 (supplementary information). For Na doping, the distinguishing peaks of Na(s) appear at -4.2, -3.8 and -0.92 eV on the left and at 0.20, 0.40 and 1.20 eV on the right of E_f . For K and Ca doping, the valence bands are mainly dominated by C(p) and B(p), with small contributions from the orbitals of K and Ca. However, at the top of E_f the hybridization of K(s) and Ca(s) with those of C(p) and B(p) are more dominated as compared to the Li and Na cases, which is evident in Figures S3 and S4, respectively.

So far we have discussed the structural, thermal stabilities, charge transfer and electronic properties, we will now move on to investigate the adsorption of H_2 on metal-functionalized BGDY monolayers. Each system has four metal dopants, which are positively charged and capable of binding H_2 molecules through electrostatic as well as van der Waals interactions. Each of the positively charged ions ($Li^{\delta+}$, $Na^{\delta+}$, $K^{\delta+}$, $Ca^{\delta+}$) generates a local electric field through which it polarizes the incoming H_2 molecules and thus induces a local negative charge on H_2 . Induction of a charge on H_2 results in a binding strength, which is much stronger than that of pristine BGDY- H_2 binding and can be calculated by the following equation:

$$E_b(H_2) = \{E(\text{BGDY}@4X:nH_2) - E(\text{BGDY}@4X) - nE(H_2)\}/n \quad (3)$$

In this equation, $E_b(H_2)$ is the binding energies of H_2 on metal functionalized BGDY, and the first, second and third terms on the right-hand-side are the total energies of BGDY@4X bonded with n H_2 molecules, pristine BGDY@4X and H_2 , respectively (where $X=Li, Na, K$ and Ca and $n=1-4$).

To avail all the active metal binding sites, we have introduced H_2 molecules on each dopant of the functionalized BGDY monolayers in a stepwise mode. That is, in the first step four H_2 molecules have been inserted on BGDY@4X and the systems are allowed to relax completely. Based on our previous experience,[12] a vertical adsorption of H_2 to the metal dopant is more favorable. In the next step, we introduced a second H_2 molecule on each dopant of the optimized BGDY@4X carrying 4 H_2 molecules. For further H_2 adsorption, a suitable distance of H_2 with the metal dopants as well as among charged induced H_2 molecules should be maintained to avoid the steric and electrostatic repulsion. Overall, each metal dopant X of BGDY@4X is bonded to two H_2 molecules, thus a total of 8 H_2 molecules have been adsorbed. This process is repeated until the systems reach saturation, that is the point where further H_2 molecules would be repelled upon optimization.

It is important to mention here that the binding energies per H_2 molecule (eq.3) is compared with the desired range of 0.15–0.60 eV/ H_2 each time an H_2 is added to the system. We have concluded that each dopant can accommodate a maximum of 4 H_2 molecules, which means that a total of 16 H_2 could be adorned on BGDY@4X with H_2 binding energies within the accepted range. The van der Waals corrected DFT $E_b(H_2)$ for all the systems with different H_2 coverage are given in Figure 3 (b). One can clearly notice a decreasing trend in the $E_b(H_2)$ values upon the increasing H_2 densities in Figure 3 (b). In case of BGDY@4Li, the binding energies vary from -0.297 to -0.170 eV per H_2 from minimum to maximum H_2 coverage. For the other dopants we obtain the following ranges of $E_b(H_2)$ per H_2 from minimum to maximum H_2 coverage: -0.343 to -0.186 (BGDY@4Na), -0.389 to -0.187 (BGDY@4K) and -0.408 to -0.206 (BGDY@4Ca) eV.

At a maximum H_2 coverage the H_2 storage capacities of 14.29, 11.11, 9.10 and 8.99 wt% have been achieved for BGDY@4Li, BGDY@4Na, BGDY@4K, BGDY@4Ca, respectively. These storage capacities are superior to those of other metal-doped monolayers such as graphene, h-BN, C_2N , GDY, MoS_2 , phosphorene and

silicene as shown in table 1. [5,10,40-44] Optimized structures of metal-functionalized BGDY under hydrogenation are given in figure 6.

For an ideal H₂ storage material, in addition to a highcontent of H₂ adsorption, desorption of H₂ molecules at feasible operating conditions is of greatimportance. Thus, it is essential to investigate the desorption capacities of H₂ under practical conditions of pressure and temperature. For this purpose, we have employed the thermodynamic analysis of the adsorption of H₂ on light metal-doped BGDY monolayers for a given temperature and pressure to understand thermodynamics of H₂. The number of H₂ molecules can be calculated from the following formula.[45, 46]

$$N_{H_2}(P, T) \propto N_0 \frac{\tilde{a} n g_n e^{n(m - \epsilon_n)/k_B T}}{\tilde{a} g_n e^{n(m - \epsilon_n)/k_B T}}, \quad (4)$$

where N_0 denotes the maximum number of adsorbed H₂ molecules, n indicates the number of H₂ molecules, μ denotes the chemical potential of the H₂ gas, and ϵ_n and g_n denote the adsorption energy per H₂ molecule and degeneracy of the configuration, respectively. The chemical potential of H₂ gas was used for the experimental values.[47] Using the Eq. (4), the number of H₂ molecules was calculated for BGDY@4X as shown in Figure 7(a). The systems GBDY@4Li and BGDY@4Na require temperature lower than the others because the E_b values of H₂ on Li and Na are smaller than that on K and Ca. In addition, the change of the number of H₂ molecules is not linearly or parabolic, that is, there are multiple flat regions as the temperature decreases. This is ascribed to the fact that the adsorption is generated from the multiple binding energy of H₂ according to the number of adsorbed H₂ molecules. On the other hand, at higher pressure the adsorption occurs at a higher temperature as shown in Figure 7(a) because the chemical potential of the H₂ gas increases as the pressure increases.[48] Thus, at constant temperature, H₂ can be released as the pressure decreases (Figure 7(b)), which is an isothermal adsorption-desorption process.

From figure 7 (a, b) it can be clearly seen that the all the systems can contain a large number of H₂ molecules at practical operating conditions of pressure and

temperature, which further confirms the effectiveness of light metal doped BGDY monolayers for high capacity H₂ storage applications.

System	Type of study	Dopants	Hydrogen Storage Capacity (wt%)	Reference
Graphene	Experimental	Pd	6.7	21
Graphene	Experimental	Ni	0.1-1.2	22
γ -graphyne	Theoretical (DFT)	Mg	10.6	23
Graphyne	Theoretical (DFT)	Li, Na	9-9.3	25
Graphdiyne	Theoretical (DFT)	Li, Na, K, Ca, Sc, Ti	4.91-6.5	5
Graphene	Theoretical (DFT)	Cu	4.23	4
C ₂ N Sheets	Theoretical (DFT)	Li	10	41
MoS ₂	Theoretical (DFT)	Li	4.4	42
Phosphorene	Theoretical (DFT)	Li	5.3	43

Table 1: Hydrogen storage capacity values from different 2D materials.

4. Conclusion:

In summary, we have employed spin-polarized DFT-D3 calculations to study the structural, electronic, charge transfer and H₂ storage properties of recently synthesized BGDY monolayers. Our simulations reveal that BGDY binds light metal dopants such as Li, Na, K and Ca with binding energies of -2.95, -2.51, -2.91, and -3.04 eV, respectively. Even at high metal doping concentrations, the metal bindings are significantly higher than the dopant's experimental cohesive energies, thus achieving a uniform metal distribution over the BGDY surface without clustering. In addition, we have also performed AIMD simulations at 400K to confirm the thermal stabilities of metal-doped BGDY monolayers. Bader charge analysis reveals that an average of 0.98, 0.68, 0.60 and 1.07 e have been transferred from Li, Na, K and Ca, respectively to the BGDY sheet, which means the dopants carry a significant positive charge. We find that each BGDY unit cell can accommodate four metal dopants of each type (Li, Na, K or Ca). These metal dopants can adsorb a maximum of 16

H₂ molecules with an average E_b (H₂) within an ideal range of $E_b = 0.17\text{--}0.40$ eV per H₂ molecule. Thus, the doped BGDY monolayer attains H₂ storage capacities which are much higher than other 2D systems reported in the literature such as graphene, graphane, graphdiyne, graphyne, C₂N, g-C₃N₄, h-BN, MXene, silicene, phosphorene. In order to design efficient H₂ storage systems, which could operate under practical operating conditions of pressure and temperature, we have studied the thermodynamic properties of metal-doped BGDY monolayers. Our comprehensive thermodynamic analysis reveals that the H₂ molecules adsorbed on the doped BGDY layer could be desorbed under practical conditions of pressure and temperature. Thus, metal functionalized BGDY is a promising material for efficient, reversible and high capacity H₂ storage under ambient conditions applications.

Acknowledgments:

This research was undertaken with the assistance of resources from the National Computational Infrastructure (NCI), which is supported by the Australian Government. AK acknowledges an Australian Research Council (ARC) Future Fellowship (FT170100373). HL was supported by the Basic Science Research Program (Grant No. KRF-2018R1D1A1B07046751) through the National Research Foundation (NRF) of Korea, funded by the Ministry of Education, Science and Technology. BM and TR acknowledge the financial support by European Research Council for COMBAT project (Grant number: 615132). BM also acknowledges *Cluster of Excellence PhoenixD (Photonics, Optics, and Engineering–Innovation Across Disciplines)*, Leibniz Universität Hannover, Hannover, Germany.

References:

1. Jena, P. Materials for hydrogen storage: past, present, and future. *J. Phys. Chem. Lett.* **2011**, 2, 206-211
2. Li, Y.; Mi, Y.; Chung, J. S.; Kang, S. G. First-principles studies of K_{1-x}M_xMgH₃ (M = Li, Na, Rb, or Cs) perovskite hydrides for hydrogen storage. *Int. J. Hydrogen Energy* **2018**, 43, 2232-2236.

3. Hussain, T.; Hankel, M.; Searles, D. J. Computational Evaluation of Lithium-Functionalized Carbon Nitride (g-C₆N₈) Monolayer as an Efficient Hydrogen Storage Material. *J. Phys. Chem. C* **2016**, 120, 25180-25188.
4. Faye, O.; Eduok, U.; Szpunar, J.; Szpunar, B.; Samoura, A.; Beye, A. Hydrogen storage on bare Cu atom and Cu-functionalized boron-doped graphene: A first principles study. *Int. J. Hydrogen Energy* **2017**, 42, 4233-4243.
5. Panigrahi, P.; Dhinakaran, A. K.; Naqvi, S. R.; Gollu, S. R.; Ahuja, R.; Hussain, T. Light metal decorated graphdiyne nanosheets for reversible hydrogen storage. *Nanotechnology* **2018**, 29, 355401-355410.
6. Mortazavi, S.Z.; Reyhani, A.; Mirershadi, S. Hydrogen storage properties of multi-walled carbon nanotubes and carbon nano-onions grown on single and bi-catalysts including Fe, Mo, Co and Ni supported by MgO. *Int. J. Hydrogen Energy* **2017**, 42, 24885-24896.
7. Mananghaya, M.; Yu, D.; Santos, G. N.; Rodulfo, E. Scandium and Titanium Containing Single-Walled Carbon Nanotubes for Hydrogen Storage: a Thermodynamic and First Principle Calculation. *Sci. Reports* **2016**, 6, 27370-27378.
8. Shen, J.; Yang, L.; Hu, K.; Luo, W.; Cheng, G. Rh nanoparticles supported on graphene as efficient catalyst for hydrolytic dehydrogenation of amine boranes for chemical hydrogen storage. *Int. J. Hydrogen Energy* **2015**, 40, 1062-1070.
9. Ensafi, A.A.; Jafari-Asl, M.; Nabiyan, A.; Rezaei, B.; Dinari, M. Hydrogen storage in hybrid of layered double hydroxides/reduced graphene oxide using spillover mechanism. *Energy* **2016**, 99, 103-114.
10. Bakhshi, F.; Farhadian, N. Co-doped graphene sheets as a novel adsorbent for hydrogen storage: DFT and DFT-D3 correction dispersion study. *Int. J. Hydrogen Energy* **2018**, 43, 8355-8364.
11. Zhou, C.; Szpunar, J. Hydrogen Storage Performance in Pd/Graphene Nanocomposites. *App. Mate. Interfaces* **2016**, 8, 25933-25940.
12. Hussain, T.; De Sarkar, A.; Ahuja, R. Functionalization of hydrogenated graphene by polyolithiated species for efficient hydrogen storage. *Int. J. Hydrogen Energy* **2014**, 39, 2560-2566.

13. Liu, Y.; Liu, W.; Wang, R.; Hao, L.; Jiao, W. *Int. J. Hydrogen Energy***2014**, 39, 12757-12764.
14. Li, C.; Li, J.; Wu, F.; Li, S-S.; Xia, J-B.; Wang, L-W.; High Capacity Hydrogen Storage in Ca Decorated Graphyne: A First-Principles Study. *J. Phys. Chem. C***2011**, 115, 23221-23225.
15. Divya, P.; Ramaprabhu, S. Hydrogen storage in platinum decorated hydrogen exfoliated graphene sheets by spillover mechanism. *Phys. Chem. Phys. Chem.* **2014**, 16, 26725-26729.
16. Lachawiec, A. J.; Qi, G.; Yang, R. T.; Hydrogen Storage in Nanostructured Carbons by Spillover: Bridge-Building Enhancement. *Langmuir***2005**, 21, 11418-11424.
17. Yadav, S.; Zhu, Z.; Singh, C. V. Defect engineering of graphene for effective hydrogen storage. *Int. J. Hydrogen Energy***2014**, 39, 4981-4995.
18. Zhou, J.; Wang, Q.; Sun, Q.; Jena, P.; Chen, X. S. Electric field enhanced hydrogen storage on polarizable materials substrates. *PNAS***2010**, 107, 2801-2806.
19. Qin, G.; Cui, Q.; Yun, B.; Sun, L.; Du, A.; Sun, Q. High capacity and reversible hydrogen storage on two-dimensional C₂N monolayer membrane. *Int. J. Hydrogen Energy***2018**, 43, 9895-9901.
20. Hussain, T.; Hankel, M.; Searles, D. J. Graphenylene Monolayers Doped with Alkali or Alkaline Earth Metals: Promising Materials for Clean Energy Storage. *J. Phys. Chem. C***2017**, **121**, 14393-14400.
21. Zhou, C.; Szpunar, J. A. Hydrogen Storage Performance in Pd/Graphene Nanocomposites. *App. Mate. Interfaces* **2016**, 8, 25933-25940.
22. Zhou, C.; Szpunar, J.; Cui, X. Synthesis of Ni/Graphene Nanocomposite for Hydrogen Storage. *App. Mate. Interfaces* **2016**, 8, 15232-15241.
23. Liu, P-P.; Zhang, H.; Cheng, H-L.; Tang, Y-J. External electric field: An effective way to prevent aggregation of Mg atoms on γ -graphyne for high hydrogen storage capacity. *App. Sur. Sci.* **2016**, 371, 44-49.
24. Pan, R.; Fan, X.; Luo, Z.; An, Y. Calcium decorated two dimensional carbon allotropes for hydrogen storage: A first-principles study. *Comp. Mate. Sci.***2016**, 124, 106-113.

25. Mohajeri, A.; ShahsavarLight metal decoration on nitrogen/sulfur codoped graphyne: An efficient strategy for designing hydrogen storage media. *Physica E Low. Dim. Sys. Nanst.* **2018**, 101, 167-173.
26. Wang, N.; Li, X.; Tu, Z.; Zhao, F.; He, J.; Guan, Z.; Huang, C.; Yi, Y.; Li, Y. Synthesis and Electronic Structure of Boron-Graphdiyne with an sp-Hybridized Carbon Skelton and Its Application in Sodium Storage. *Angew Chem. Int. Ed* **2018**, 57, 3968-3973.
27. Mortazavi, B.; Shahrokhi, M.; Zhuang, X.; Rabczuk, T. Boron–graphdiyne: a superstretchable semiconductor with low thermal conductivity and ultrahigh capacity for Li, Na and Ca ion storage. *J. Mat. Chem. A* **2018**, 6, 11022-11036.
28. Kresse, G.; Hafner, J. Ab initio molecular dynamics for liquid metals. *Phys. Rev. B* **1993**, 47, 558-561.
29. Kresse, G.; Hafner, J. Ab initio molecular-dynamics simulation of the liquid-metal–amorphous-semiconductor transition in germanium. *Phys. Rev. B* **1994**, 49 14251-14269.
30. Perdew, J. P.; Burke, K.; Ernzerhof, M. Generalized gradient approximation made simple. *Phys. Rev. Lett.* **1996**, 77, 3865-3868.
31. Blochl, P. E. Projector augmented-wave method. *Phys. Rev. B* **1994**, 50, 17953-17979.
32. Grimme, S.; Antony, J.; Ehrlich, S.; Krieg, H. A consistent and accurate ab initio parametrization of density functional dispersion correction (DFT-D) for the 94 elements H–Pu. *J. Chem. Phys.* **2010**, 132, 154104-154119.
33. Monkhorst, H. J.; Pack, J. D. Special points for Brillouin-zone integrations. *Phys. Rev. B* **1976**, 13, 5188-5192.
34. Bader, R. F. W., *Atoms in Molecules - a Quantum Theory*, Oxford University Press, Oxford, **1990**.
35. Yu, Y. X. Graphenylene: a Promising Anode Material for Lithium-ion Batteries with High Mobility and Storage. *J. Mater. Chem. A* **2013**, 1, 13559–13566.
36. Chan, K. T.; Neaton, J. B.; Cohen, M. L. First-Principles Study of Metal Adatom Adsorption on Graphene. *Phys. Rev. B: Condens. Matter Mater. Phys.* **2008**, 77, 235430–23541.

37. Naqvi, S. T.; Hussain, T.; Luo, W.; Ahuja, R. Metallized siligraphene nanosheets (SiC₇) as high capacity hydrogen storage materials. *Nano Research***2013**, 11, 3802-3813.
38. Kulish, V. V.; Malyi, O. I.; Persson, C.; Wu, P. Adsorption of metal adatoms on single-layer phosphorene. *Phys. Chem. Chem. Phys.* **2015**, 17, 992-1000.
39. Naqvi, S. T.; Hussain, T.; Luo, W.; Ahuja, R. Exploring Doping Characteristics of Various Adatoms on Single-Layer Stanene. *J. Phys. Chem. C***2017**, 121, 7667-7676.
40. Hussain, T.; Islam, M. S.; Rao, G. S. Panigrahi, P.; Gupta D. Ahuja, R. Hydrogen storage properties of light metal adatoms (Li, Na) decorated fluorographene monolayer. *Nanotechnology***2015**, 26, 275401-275406.
41. Hashmi, A.; Farooq, M. U.; Khan, I.; Son, J.; Hong, J. Ultra-high capacity hydrogen storage in a Li decorated two-dimensional C₂N layer. *J. Mat. Chem. A***2017**, 5, 2821-2828.
42. Putugan, D. B.; Lin, S-H.; Wei, C-M.; Kuo, J-L. Li adsorption, hydrogen storage and dissociation using monolayer MoS₂: an *ab initio* random structure searching approach. *Phys. Chem. Phys. Chem.* **2015**, 17, 11367-11374.
43. Haldar, S.; Mukherjee, S.; Ahmed, F.; Singh, C. V. A first principles study on hydrogen storage in lithium decorated defected phosphorene. *Int. J. Hydrogen Energy***2017**, 42, 23018-23027.
44. Wang, Y.; Zheng, R.; Gao, H.; Zhang, J.; Xu, B.; Sun, Q.; Jia, Y. Metal adatoms-decorated silicene as hydrogen storage media. *Int. J. Hydrogen Energy***2014**, 39, 14027-14032.
45. Lee, H.; WI Choi, W. I.; Ihm, J. Combinatorial search for optimal hydrogen-storage nanomaterials based on polymers, *Phys. Rev. Lett.* **2006**, 97, 056104-056107.
46. Hwang, H. J.; Kwon, Y.; Lee, H. Thermodynamically stable calcium-decorated graphyne as a hydrogen storage medium, *J. Phys. Chem. C***2012**, 116, 20220-20224.
47. The chemical potential of gases, $\mu = (H - TS)/N$, where H, S, and N denote the enthalpy, the entropy, and the number of particles was calculated from the data of the enthalpy (H) and entropy (S) in the reference:
<http://webbook.nist.gov/chemistry/fluid/>.

48. Lee, H.; Choi, W. I.; Nguyen, M. C.; Cha, M-H.; Moon, E.; Ihm, J. Ab initio study of dihydrogen binding in metal-decorated polyacetylene for hydrogen storage. *Phys. Rev. B* **2007**, 76, 195110-195116.

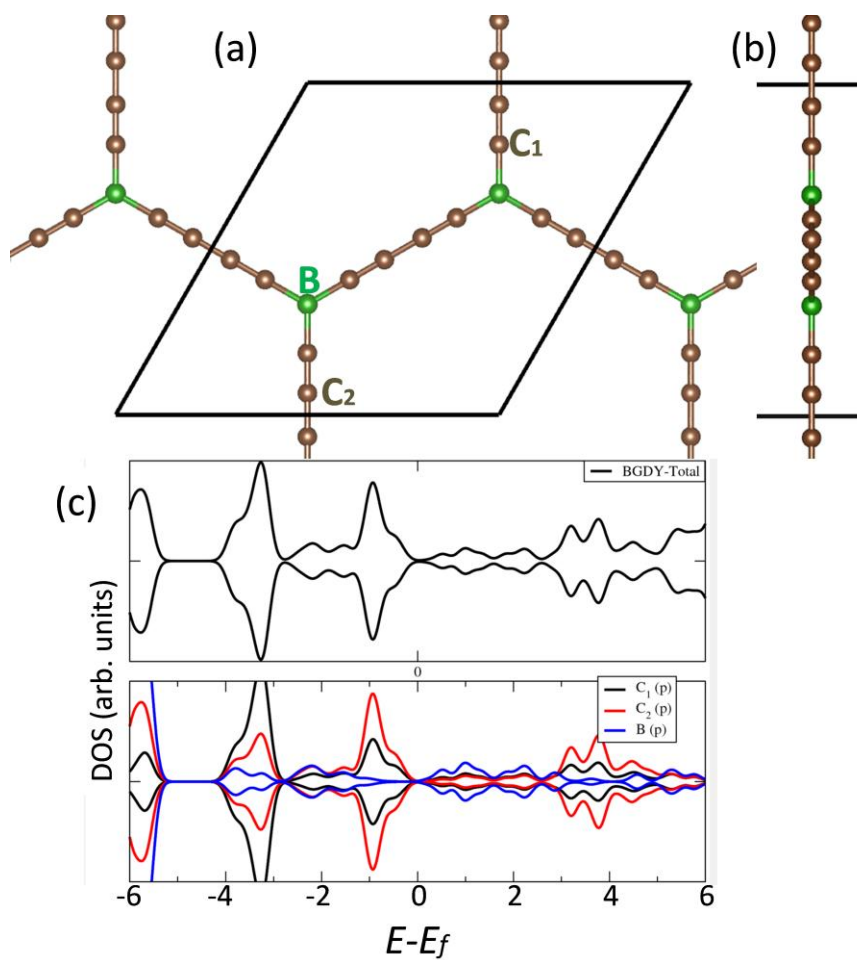


Figure 1. Top (a) and side (b) view of ground state configuration of BGDY monolayer. Brown and green balls represent C and B atoms, respectively. Total and partial densities of states plots are also given in (c).

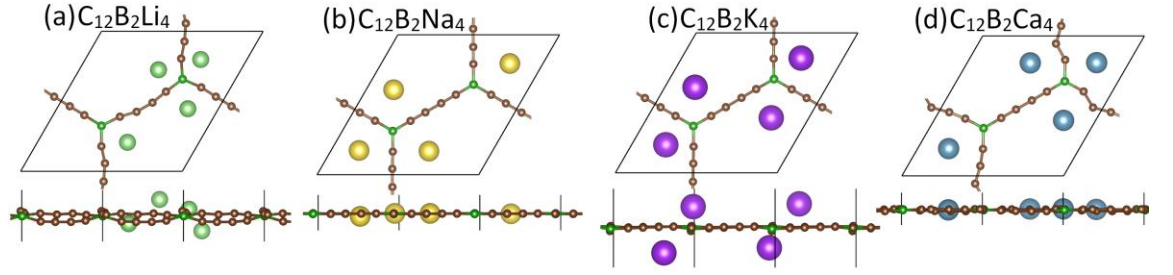


Figure 2. Top and side views of the optimized structures of (a) BGDY@4Li, (b) BGDY@4Na, (c) BGDY@4K and (d) BGDY@4Ca. Brown, dark green, light green, yellow, purple and blue atoms represent C, B, Li, Na, K and Ca, respectively.

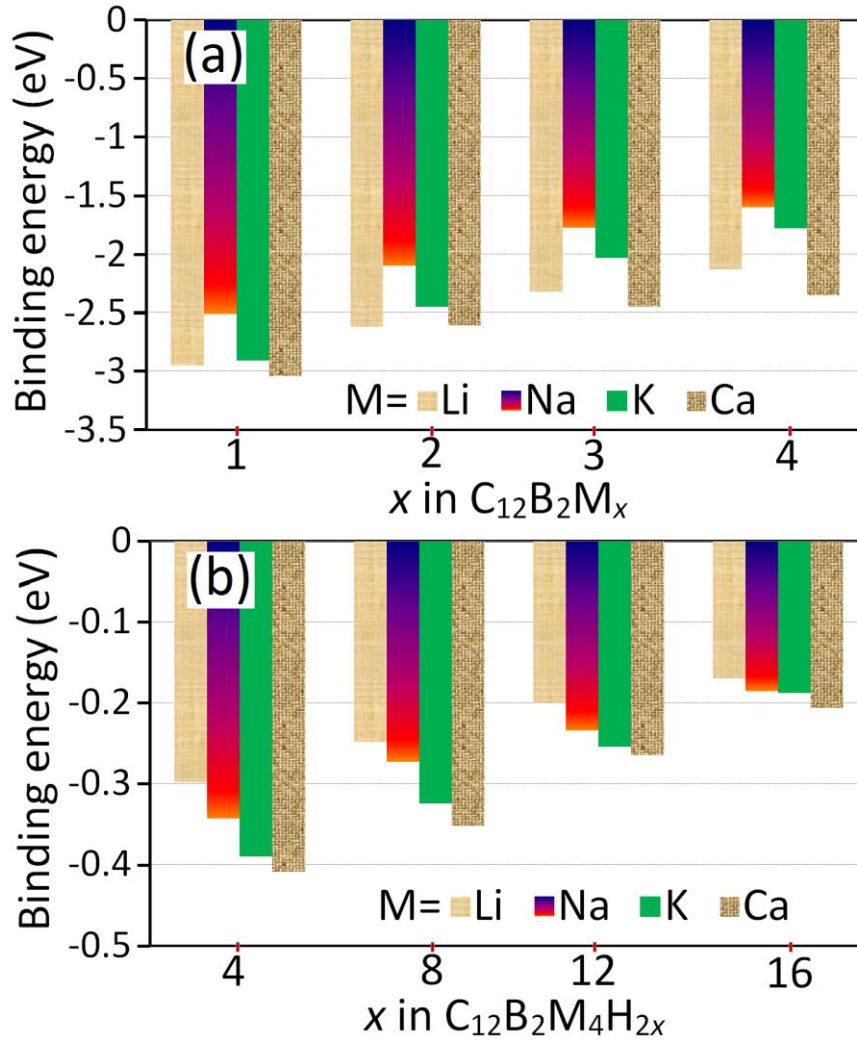


Figure 3. (a) Binding energies (E_b) of metal dopants over BGDY monolayer at different doping concentrations. (b) Average H_2 adsorption energies (per H_2 molecule) on BGDY loaded with four metal dopants.

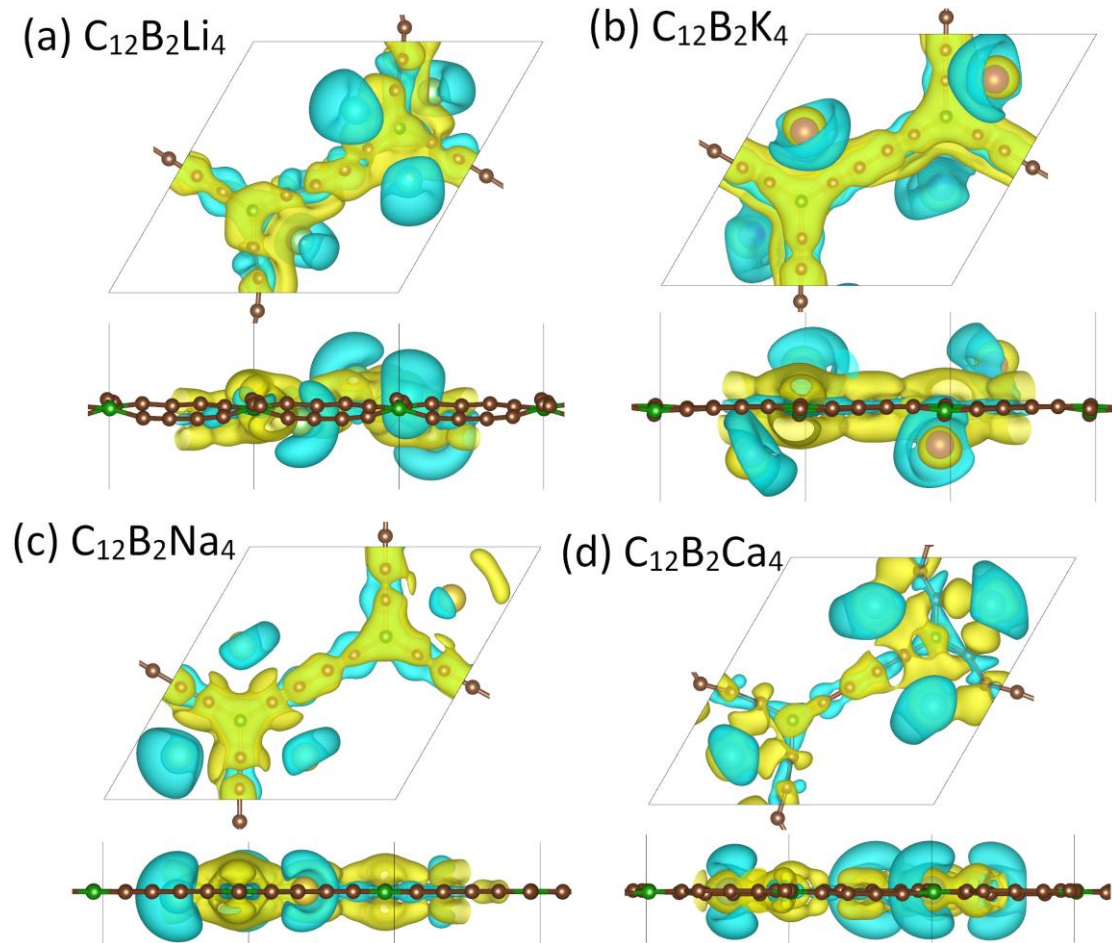


Figure 4. Isosurface charge densities of Li, Na, K and Ca doped BGDY monolayers at maximum doping concentrations with isovalue of $0.01 \text{ e}/\text{\AA}^3$. Yellow and cyan surfaces indicate the accumulation and depletion of charges, respectively.

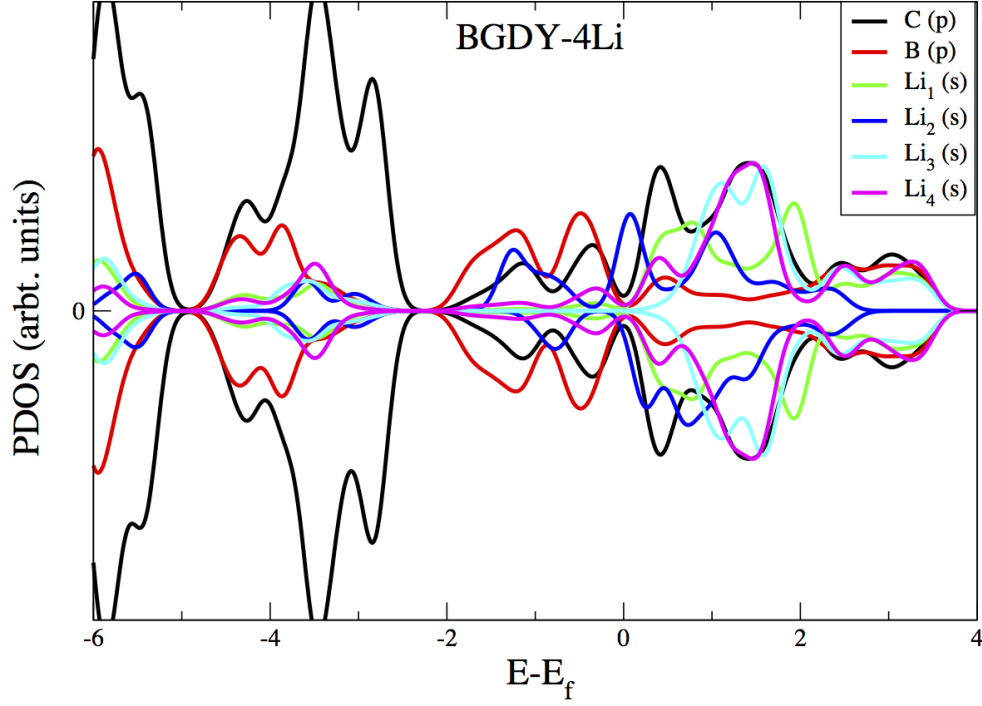


Figure 5. PDOS plots of BGDY-4Li monolayer. The Fermi level is set to zero.

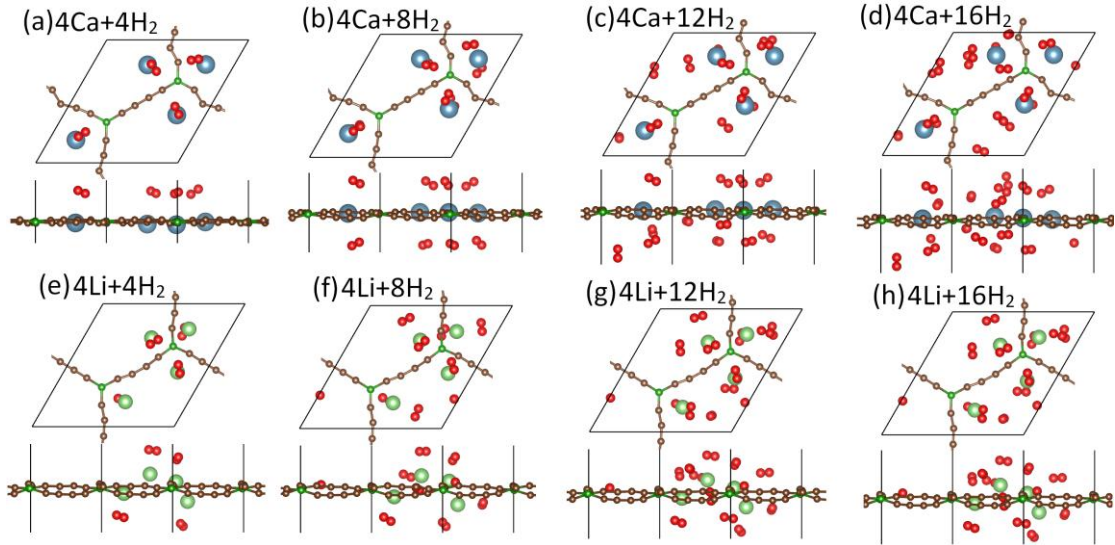


Figure 6. Top and side views of the optimized structures of (a-d) BGDY@4Ca and (e-h) BGDY@4Li loaded with 4H₂, 8H₂, 12H₂ and 16H₂, respectively. Brown, dark green, blue, light green, and red atoms represent C, B, Ca, Li and H, respectively.

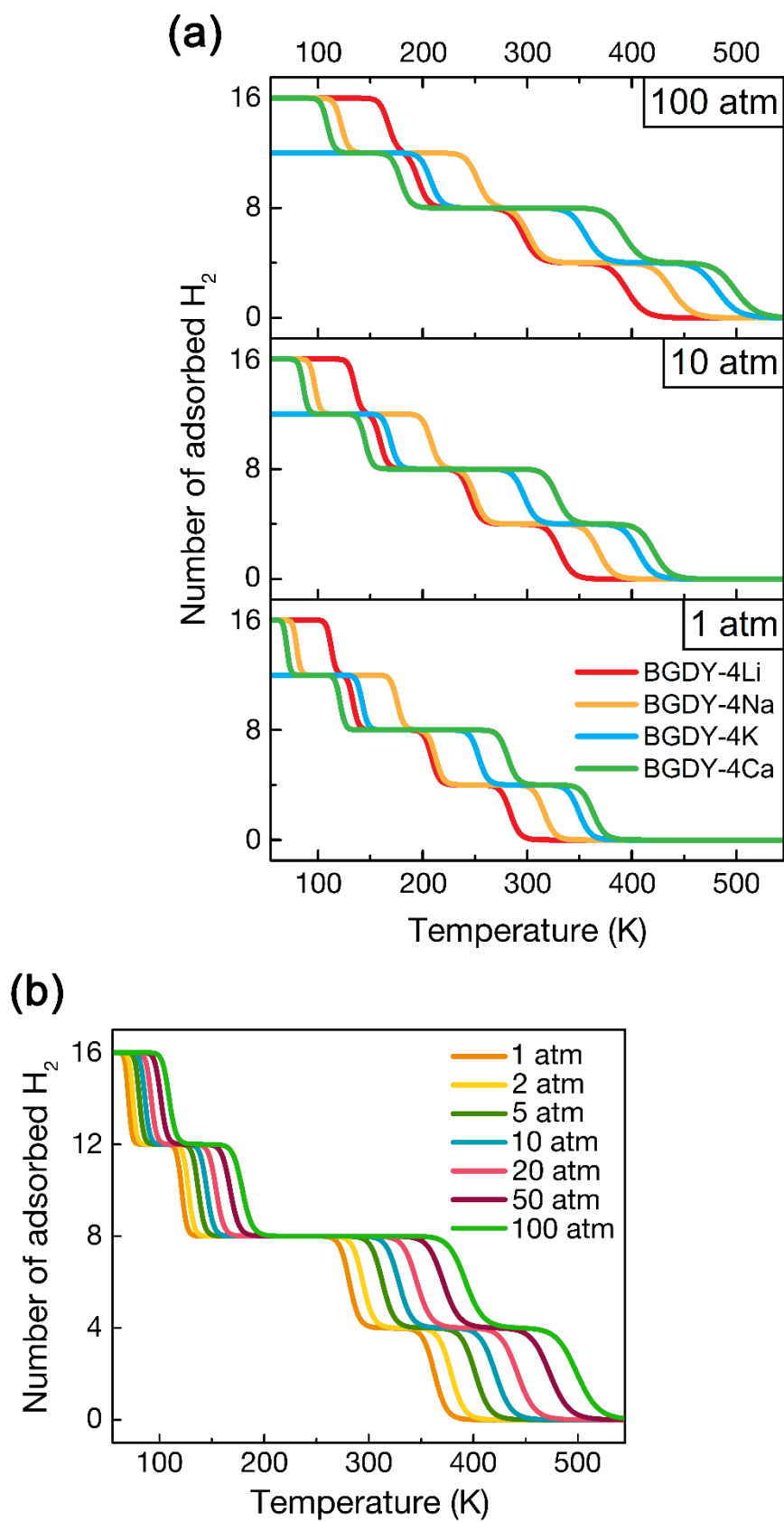


Figure 7. The thermodynamics of H_2 adsorption on alkali-metal-doped BGDY. (a) The adsorption of H_2 molecules on alkali-metal-doped BGDYs, as a function of the

temperature and the pressure of H₂ gas. (b) Adsorption-desorption process by changing pressure of H₂, for BGDY-4Ca.

System	E _b per X (eV)	E _b /E _c	D ₁ (Å) X-BGDY distance	D ₂ (Å) X-X distance	Charge transferred Q (e)
BGDY-Li	-2.95	1.81	2.10	11.84	0.992
BGDY-2Li	-2.62	1.60	2.16	6.02	0.991
BGDY-3Li	-2.32	1.42	2.20	4.83	0.987
BGDY-4Li	-2.13	1.29	2.29	4.45	0.980
BGDY-Na	-2.51	2.61	2.39	11.84	0.992
BGDY-2Na	-2.10	1.89	2.43	5.93	0.991
BGDY-3Na	-1.77	1.59	2.53	5.88	0.747
BGDY-4Na	-1.60	1.44	2.58	5.16	0.680
BGDY-K	-2.91	3.13	2.73	11.84	0.914
BGDY-2K	-2.45	2.63	2.80	6.79	0.893
BGDY-3K	-2.03	2.18	2.81	5.81	0.727
BGDY-4K	-1.78	1.91	2.85	5.20	0.600
BGDY-Ca	-3.04	1.65	2.39	11.84	1.459
BGDY-2Ca	-2.61	1.41	2.46	8.71	1.139
BGDY-3Ca	-2.44	1.32	2.40	5.45	1.107
BGDY-4Ca	-2.35	1.27	2.48	4.86	1.070

Table 1. Binding energies (E_b), binding to cohesive energies ratio (E_b/E_c), average dopants-BGDY distance (D₁), average dopant-dopant distance (D₂) and average charge transferred from dopants to BGDY monolayers (Q). X=Li, Na, K, Ca